Theoret. Appl. Mech., Vol.35, No.1-3, pp. 137–170, Belgrade 2008

Elastoplastic damage micromechanics for elliptical fiber composites with progressive partial fiber debonding and thermal residual stresses

J.W. Ju * **K. Yanase** †

Abstract

Incorporating the interfacial damage and thermal residual stresses, an elastoplastic damage formulation is proposed to predict the overall transverse mechanical behavior of continuous elliptical-fiber reinforced ductile matrix composites within the framework of micromechanics and homogenization. Based on the concept of equivalent inclusion and taking the progressive interfacial debonding angle into consideration, partially debonded fibers are replaced by equivalent orthotropic, perfectly bonded fibers. Three interfacial damage modes are considered. The Weibull's probabilistic function is adopted to describe the varying probability of progressive partial fiber debonding. The effective elastic moduli of four-phase composites, composed of a ductile matrix and randomly located yet unidirectionally aligned fibers are derived by a micromechanical formulation.

Thermal residual stresses are taken into account through the concept of thermal eigenstrain to investigate the effects of the manufacturing process-induced residual stresses. Employing the micromechanical approximation, the overall stress-strain responses and the effective yield function are formulated with the thermal eigenstrain. When comparing with the available experimental data, significant effects of thermal residual stresses are discussed. Moreover, the effects of the interfacial strengths and the cross-sectional shapes of fibers on the mechanical behaviors of composites are systematically investigated.

Keywords: Elliptical fiber reinforced composites, metal matrix composites, probabilistic micromechanics, damage mechanics, interfacial debonding, residual stress, homogenization

*Department of Civil and Environmental Engineering, University of California, Los Angeles, CA 90095-1593, USA, e-mail:juj@ucla.edu

†Department of Civil and Environmental Engineering, University of California, Los Angeles, CA 90095-1593, USA

1 Introduction

The requirement for higher structural efficiency (a combination of stiffness and strength normalized by density) provides a significant motivation for the development of improved materials for a multitude of engineering applications. Composite materials have been widely studied and employed in diverse fields of science and engineering disciplines. In comparison with many conventional materials (such as steel and aluminum), fiber- or particle-reinforced composites offer salient features such as low density, high strength-to-weight ratio, high stiffness, high toughness, improved creep resistance, enhanced wear resistance, superior environmental durability, custom microstructure-morphology, and preferred directionality, etc. The matrix material may consist of metal, ceramic or polymer. The inclusions encompass unidirectionally aligned, bi-directional, or randomly dispersed in a matrix material. Among various types, continuous fiber reinforced composites often serve as the basic building block. Moreover, continuous fiber reinforced composites are attractive as they offer outstanding longitudinal mechanical properties compared with composites reinforced by particulates or whiskers.

Structurally efficient metallic materials provide a direct path for reducing mass, thus improving the performance of structural components (Tamirisakandala et al., 2004). Metal matrix composites (MMCs) are a class of materials in which stiffer (ceramic) reinforcements are embedded in a ductile metal or alloy matrix. By taking advantages of metallic properties (ductility and toughness) and ceramic characteristics (high strength and modulus), MMCs can provide greater strength and higher service temperature capabilities. The attractive physical and mechanical properties of MMCs, have lead to extensive use in the aerospace and automotive industries, and in other structural applications over the past two decades.

The mechanical behavior of MMCs is sensitive to temperature changes. Firstly, the material properties of MMCs are dependent upon temperatures. Secondly, thermal residual stresses normally exist in the composites due to the high temperature fabrication/annealing and subsequent cooling process. Although the introduction of rigid inhomogeneity improves the material properties of matrix, simultaneously, their existence induces the thermal residual stresses in MMCs due to the mismatch of the coefficients of thermal expansions (CTEs) between the matrix and inhomogeneity. Since the CTE of the matrix is usually greater than that of inhomogeneity, the differential thermal contraction results in the internal *tensile* stress in the matrix and *compressive* stress in the inhomogeneity. Residual stress can be detrimental when it reduces the tolerance of material to an external loading. Beneficial residual stresses can also be introduced deliberately; a good example of this is the toughened glass (Withers and Bhadeshia, 2001a,b). In advanced composite systems, the residual stress states at the room temperature can be large and may damage the composites even prior to the first external mechanical loading.

In the literature, extensive research has been implemented to understand the effects of thermal residual stresses on the effective thermomechanical behaviors of MMCs. The majority of analytical models are based on the Eshelby's (1957) equivalence principle, aiming at the analysis of a representative volume element (RVE) or area element (RAE) in which the reinforcements are randomly distributed. The main advantage of Eshelby's approach is that it enables us to predict the full multiaxial properties and responses of heterogeneous materials, which are often difficult to measure experimentally. The Eshelby's approach has been extensively used to predict the effective mechanical properties of composites (e.g., Hill, 1965; Mori and Tanaka, 1973; MacLaughlin, 1977; Christensen and Lo; 1979, Weng, 1984; Norris, 1985; Ju and Chen, 1994a,b,c; Ju and Zhang, 1998, 2001; Ju and Sun, 2001; Sun and Ju, 2001, 2004). Regarding the thermal effects, the asymmetry in tensile/compressive yield strengths due to residual stresses were studied for whisker (Withers et al., 1989), particle (Povirk et al., 1991; Hu and Weng, 1998; Liu and Sun, 2004) and long-fiber (Arsenault and Taya, 1987) reinforced composites. The use of finite element method (unit cell) to investigate the thermomechanical behaviors of MMCs is also popular. Levy and Papazian (1991) and Davis and Allison (1993) discussed the residual stresses in MMCs after cooling, and Levy and Papazian (1993) investigated the effects of thermal cycling. Aghdam and Falahatgar (2004) studied the effects of residual stress, fiber coating, and interface bonding on the transverse behavior of unidirectional SiC/Ti-6Al-4V MMCs.

The interfacial debonding is a predominant damage mode for the composites; the evolution of interfacial damage is dictated by the local stress and strain fields at the interfaces between the reinforcing phase and matrix. In the literature, the influences of thermal residual stresses upon the interfacial debonding were investigated theoretically and experimentally, for the whisker reinforced (Zhou et al., 2000) and fiber reinforced composites (Nimmer et al., 1991; Gundel et al., 1995, 1999; Warrier et al., 1999; Naboulsi, 2003). In Eshelby's celebrated work, it is assumed that inclusion or inhomogeneity is perfectly bonded to the matrix. However, in many engineering applications, the interfaces in a composite material may not be perfectly bonded. Inhomogeneities in high strength steel are easily debonded after some cycles of loading. Grain boundary sliding in polycrystals and granular materials are common phenomena. Defects and damage may develop on the interfaces of composites, resulting in imperfect interfaces.

The transverse properties of continuous-fiber reinforced composites depend upon the ability of the interfaces to transfer the loads from the matrix to fibers. The weak interfaces lead to the fiber/matrix debonding under transverse loading, which in turn severely reduces the transverse strengths. The strength in the transverse direction with significant interfacial fiber debonding is often less than that of the matrix material. It is often the transverse mechanical properties and strengths that limit the use of such composite materials in practical applications.

In order to tackle the problems related to the interfacial damage, micromechanics has been extensively used, and various models have been proposed. The first type of models can be referred to as the *interface* models, in which the presence of displacement and traction discontinuities are assumed at the interface, such as the free-sliding model and linear-spring model. The free-sliding model allows the relative slip in the tangential direction of the inhomogeneity but does not admit the displacement jump in the normal direction at the interface. Physically, the free-sliding model may represent the grain boundary sliding in polycrystals, behavior of precipitates at high temperature, or imperfectly bonded interfaces in composites. The free-sliding model was employed to analyze the local elastic fields and effective properties by Ghahremani (1980), Mura and Furuhashi (1984), and Jasiuk et al. (1987). In the linear-spring model, the imperfection of interface is reflected mainly by the discontinuity of displacement field across the interface. The linear-spring model postulates that the traction is continuous across the interface but the displacement field is discontinuous; the related eigenstrain problem is called the modified Eshelby inclusion problem (Qu and Cherkaoui, 2006). The linear-spring model was used to study the stress fields in composites by many researchers (e.g., Aboudi, 1987; Hashin, 1991; Qu, 1993a,b; Gao, 1995; Zhong and Meguid, 1997; Shen at al., 2000; Duan et al., 2005).

The second type of models is called the *interphase* models, which describes the interface region as a layer between the inhomogeneity and matrix. This interphase layer has a given thickness and distinct elastic moduli from the inhomogeneity and matrix; perfect bonding is usually assumed at both the matrix/interphase and inhomogeneity/interphase, enabling the modeling of composites with coated inhomogeneities (cf., Li et al., 1999; Hashin, 2002; Hashin and Monteiro, 2003; Heukamp et al., 2005).

The interface damage/failure is primarily responsible for the stiffness reduction of certain metal and polymer matrix composites under static or cyclic loading due to the loss of load transfer ability of reinforcements. Accordingly, in the third type of models, known as the method of equivalent inclusion, the debonded particles/fibers in various stages of partial debonding modes are treated as a distinct phase of perfectly bonded yet anisotropic particles/fibers with reduced moduli. Zhao and Weng (1997, 2002) investigated the effects of partial debonding and the associated debonding angle on effective properties of composites. By combining with probability function (Weibull, 1951; Rinaldi et al., 2007), the method of equivalent inclusion was further adopted to study the behaviors of particle reinforced (Liu et al., 2004, 2006) and fiber reinforced MMCs (Ju and Lee, 2000, 2001; Ju et al., 2006; Ju and Yanase, 2007).

The main objective of present paper is to develop a multi-stage elastoplastic-damage micromechanical formulation with progressive interfacial partial debonding and prescribed thermal eigenstrain, for elliptical-fiber reinforced ductile matrix

composites under transverse loading. The fibers are assumed to be elastic, randomly located in the matrix and unidirectionally aligned. The ductile matrix behaves elastoplastically under arbitrary transverse loading. Once the composites are loaded to a certain level, interfacial fiber debonding may develop. The effective properties of the four-phase composites are statistically homogeneous and orthotropic, via the equivalent inclusion method and three interfacial damage modes. The Weibull's probability is adopted to characterize the varying probability of progressive partial fiber debonding. An effective yield function is micromechanically derived under the presence of residual stresses to capture the overall elastoplastic damage behavior of composites.

2 Effective elastic moduli of multi-phase composites

2.1 The concept of equivalent inclusion approach

The progressive interfacial debonding process gradually reduces the overall elastic properties of composites. This is mainly due to the progressive loss of load transfer capability between the matrix and fibers, caused by damaged interfaces. The extent of reduction depends on the debonding geometry. To tackle the issues related to the interfacial damage, some theories were developed in the literature. For instance, Zhao and Weng (1997, 2002) developed a concept of equivalent inclusion to simulate the behavior of partially debonded inclusions. Under the assumption of perfectly-bonded inclusions, the Eshelby's equivalence principle can be directly implemented without re-deriving the Eshelby tensor. Further, Zheng et al. (2003) demonstrated that the debonding angle is a dominant damage parameter in estimating the effective moduli of composites and that equivalent inclusion can reproduce good results for the composite stiffness and behavior in comparison with the finite element analysis.

Emanating from the notion that the tensile radial stress at the interface controls the interfacial debonding initiation and as the tensile radial stress reaches a critical interfacial debonding stress σ_{cri}, the local debonding criterion can be characterized as

$$\begin{array}{l} \sigma^{Interface} \geqslant \sigma_{cri} \text{ , then the interface is partially debonded.} \\ \sigma^{Interface} < \sigma_{cri} \text{ , then the interface is perfectly bonded.} \end{array} \tag{1}$$

Since thermal residual stresses are induced before mechanical loading due to the manufacturing process, the presence of residual stresses plays an important role for the interfacial damage evolution in addition to mechanical loading in Eq.(1).

Eigenstrain is introduced in micromechanics to represent inelastic strains such as thermal strain, phase transformation stain, plastic strain, and misfit strain

(Mura, 1987; Qu and Cherkaoui, 2006). The temperature change of composite during manufacturing process generates a misfit between the natural shape of the inclusion and the corresponding matrix. By subtracting the strain of matrix from that of inclusion, the effect of temperature change ΔT can be simulated by the differential thermal contraction misfit (Withers et al., 1989; Clyne and Withers, 1993) as:

$$\overset{*}{\varepsilon}_{Th} = (\alpha_1 - \alpha_0)\Delta T \delta_{ij} \tag{2}$$

Here, α_0 and α_1 signify the coefficients of thermal expansion (CTE) of the matrix and inclusion, respectively, and δ_{ij} is the Kronecker delta. Since the thermal eigenstrain is the stress-free strain in the inclusion, the Eshelby's equivalence principle leads to the total eigenstrain ε^*_{Total}:

$$\mathbf{C}^{(1)} : (\varepsilon^o + \varepsilon^{'} - \varepsilon^*_{Th}) = \mathbf{C}_0 : (\varepsilon^o + \varepsilon^{'} - \varepsilon^*_{Total}) \tag{3}$$

$$\varepsilon^*_{Total} = (\mathbf{A}_1 + \mathbf{S})^{-1} : (\mathbf{B}_1 : \varepsilon^*_{Th} - \varepsilon^o) \tag{4}$$

where

$$\begin{aligned} \mathbf{A}_1 &= (\mathbf{C}^{(1)} - \mathbf{C}_0)^{-1} \bullet \mathbf{C}_0 \\ \mathbf{B}_1 &= (\mathbf{C}^{(1)} - \mathbf{C}_0)^{-1} \bullet \mathbf{C}^{(1)} \end{aligned} \tag{5}$$

where $\mathbf{C}_0$, $\mathbf{C}^{(1)}$ represent the stiffness tensors of the matrix and the perfectly bonded fiber, respectively. Furthermore, $\varepsilon^{\mathbf{o}}$, ε' signify the far field and perturbed strain fields; $\mathbf{S}$ represents the interior-point Eshelby's tensor for an elliptical fiber (cf. Mura, 1987; Nemat-Nasser and Hori, 1993; Ju and Sun, 2001). In addition, "$\bullet$" denotes the 4^{th}-order tensor multiplication. The elastic stiffness of the perfectly bonded fiber can be written as

$$C^{(1)}_{ijkl} = \lambda^{(1)}\delta_{ij}\delta_{kl} + \mu^{(1)}(\delta_{ik}\delta_{jl} + \delta_{il}\delta_{jk}), \quad i,j,k,l = 1,2,3 \tag{6}$$

where $\lambda^{(1)}$ and $\mu^{(1)}$ denote the isotropic Lamé constants of the perfectly bonded fibers. The components of the Eshelby's tensor $\mathbf{S}$ for an elliptical fiber are given as follows:

$$S_{ijkl} = \frac{1}{4(1-\nu_0)}\{S^{(1)}_{IK}\delta_{ij}\delta_{kl} + S^{(2)}_{IJ}(\delta_{ik}\delta_{jl} + \delta_{il}\delta_{jk})\}, \quad i,j,k,l = 1,2,3 \tag{7}$$

$$\begin{aligned} S^{(1)}_{11} &= 2\left\{-\frac{(1-2\nu_0)\alpha}{1+\alpha} + \frac{1}{3}\left[1 - \frac{1}{(1+\alpha)^2}\right]\right\}, \\ S^{(1)}_{22} &= 2\left\{-\frac{1-2\nu_0}{1+\alpha} + \frac{1}{3}\left[1 - \frac{\alpha^2}{(1+\alpha)^2}\right]\right\} \\ S^{(1)}_{33} &= 0, \end{aligned} \tag{8}$$

$$S^{(1)}_{12} = 2\left\{\frac{\alpha^2}{(1+\alpha)^2} - \frac{(1-2\nu_0)\alpha}{\alpha+1}\right\}, \quad S^{(1)}_{21} = 2\left\{\frac{1}{(1+\alpha)^2} - \frac{(1-2\nu_0)}{\alpha+1}\right\} \tag{9}$$

$$S_{23}^{(1)} = \frac{4\,\nu_0}{1+\alpha}, \quad S_{32}^{(1)} = 0, \quad S_{13}^{(1)} = \frac{4\,\nu_0\alpha}{1+\alpha}, \quad S_{31}^{(1)} = 0 \tag{10}$$

$$S_{11}^{(2)} = 2\left\{\frac{(1-2\nu_0)\alpha}{1+\alpha} + \frac{1}{3}\left[1 - \frac{1}{(1+\alpha)^2}\right]\right\},$$

$$S_{22}^{(2)} = 2\left\{\frac{1-2\nu_0}{1+\alpha} + \frac{1}{3}\left[1 - \frac{\alpha^2}{(1+\alpha)^2}\right]\right\} \tag{11}$$

$$S_{33}^{(2)} = 0, \quad S_{12}^{(2)} = 2\left\{(1-\nu_0) - \frac{\alpha}{(\alpha+1)^2}\right\}, \quad S_{21}^{(2)} = S_{12}^{(2)} \tag{12}$$

$$S_{23}^{(2)} = \frac{2\,(1-\nu_0)}{1+\alpha}, \quad S_{32}^{(2)} = S_{23}^{(2)}, \quad S_{13}^{(2)} = \frac{2\,(1-\nu_0)\,\alpha}{1+\alpha}, \quad S_{31}^{(2)} = S_{13}^{(2)} \tag{13}$$

where $\alpha = a_2/a_1$ is the aspect ratio of an elliptical fiber and ν_0 is the matrix Poisson's ratio.

By making use of the Eshelby's theory associated with the total eigenstrain without the near-field interactions among the inclusion-phase, the interfacial stress of the perfectly bonded fiber (cf. Ju, Ko and Zhang, 2008) can be approximated not only as a function of macrostress $\bar{\sigma}$ but as a function of prescribed thermal eigenstrain ε_{Th}^{*} that is directly related to the temperature change:

$$\sigma^{Interface} = \mathbf{F} : \bar{\sigma} + \mathbf{G} : \varepsilon_{Th}^{*} \tag{14}$$

where

$$\mathbf{F} = \mathbf{C}_0 \bullet \left\{(\mathbf{I}+\phi\overline{\overline{\mathbf{A}}})^{-1}+(\mathbf{I}-\mathbf{S}) \bullet \bar{\mathbf{A}} \bullet (\mathbf{I}+\phi\overline{\overline{\mathbf{A}}})^{-1}\right\} \bullet \mathbf{C}_0^{-1} \tag{15}$$

$$\mathbf{G} = \mathbf{C}_0 \bullet \left\{\phi(\mathbf{I}+\phi\overline{\overline{\mathbf{A}}})^{-1} \bullet \overline{\overline{\mathbf{A}}} - (\mathbf{I}-\mathbf{S}) \bullet \left[\bar{\mathbf{A}} - \phi\bar{\mathbf{A}} \bullet (\mathbf{I}+\phi\overline{\overline{\mathbf{A}}})^{-1} \bullet \overline{\overline{\mathbf{A}}}\right]\right\} \bullet \mathbf{B}_1 \tag{16}$$

$$\bar{\mathbf{A}} = (\mathbf{A}_1+\mathbf{S})^{-1} \quad ; \quad \overline{\overline{\mathbf{A}}} = (\mathbf{I}-\mathbf{S}) \bullet (\mathbf{A}_1+\mathbf{S})^{-1} \tag{17}$$

Eq.(14) clearly demonstrates that the residual stress or the temperature change affects the interfacial stress, thus interfacial damage evolution. Further, if the thermal effect is neglected**,** Eq.(14) reduces to the formulation for interface stress without thermal effects (Ju and Yanase, 2007). The fourth-rank tensor $\mathbf{F}$ represents the stress concentration factor, and is obtained by assuming that the interface sliding induced by tangential shear is absent. However, it is suggested that, in composites with weak interface, the interface sliding precedes the interface separation or debonding in the normal direction. Under such circumstances, the stress concentration factor is increased by a multiplication factor β, which ranges from unity (no sliding) to 1.34 (free interface sliding), Therefore, Eq.(14) becomes:

$$\sigma^{Interface} = \beta \cdot \mathbf{F} : \bar{\sigma} + \mathbf{G} : \varepsilon_{Th}^{*} \tag{18}$$

In order to calculate β, the coefficient of interfacial friction under tangential shear need to be determined by experiment. In the present study, a value of 1.1 is adopted for β to account for the effect of shear sliding; cf. Warrier et al.(1997).

Although failure may initiate by the shear sliding prior to the interface separation, the displacement associated with shear sliding is insignificant in a transverse stress-strain relation. Moreover, based on the finite element analysis, Warrier et al. (1997) demonstrated that initiation of nonlinearity in the transverse stress-strain curve is associated with the interface separation. The significant effect of shear sliding prior to interface separation is the stress-redistribution, which results in the increase of the stress concentration factor.

Figure 1 shows the interfacial debonding geometry for an elliptical fiber, with a_1 and a_2 denoting the principal semi-axes and r the radius; $\hat{n}_1$ and $\hat{n}_2$ are the components of the unit outward normal vector $\hat{n}$ located at the fiber/matrix interface. Geometrically, we can write:

$$\hat{n}_1 = \frac{\dfrac{x_1}{a_1^2}}{\sqrt{\left(\dfrac{x_1}{a_1^2}\right)^2 + \left(\dfrac{x_2}{a_2^2}\right)^2}} \;\; ; \;\; \hat{n}_2 = \frac{\dfrac{x_2}{a_2^2}}{\sqrt{\left(\dfrac{x_1}{a_1^2}\right)^2 + \left(\dfrac{x_2}{a_2^2}\right)^2}};$$

$$r(\theta) = \frac{a_1\, a_2}{\sqrt{a_2^2 \cos^2\theta + a_1^2 \sin^2\theta}} \tag{19}$$

The relation between the local radial stresses and the critical debonding stress defines the local partial fiber debonding initiation criterion:

$$\sigma_{11}^{Interface} \cdot \hat{n}_1^2 + \sigma_{22}^{Interface} \cdot \hat{n}_2^2 = \sigma_{cri} \tag{20}$$

Therefore, we arrive at the following three different types of interfacial debonding modes.

Mode 1: $\sigma_{cri} > \sigma_{11}^{Interface} > \sigma_{22}^{Interface}$

All elliptical fibers are perfectly bonded due to the fact that none of the local radial stresses reaches the critical debonding stress. As a result, no partial debonding process is activated.

Mode 2: $\sigma_{11}^{Interface} > \sigma_{cri} > \sigma_{22}^{Interface}$

Only one local radial stress component exceeds the critical interfacial debonding strength σ_{cri}. In this case, the interfacial partial debonding initiates from the 1-direction and propagates toward the 2-direction. The debonding angle θ can be

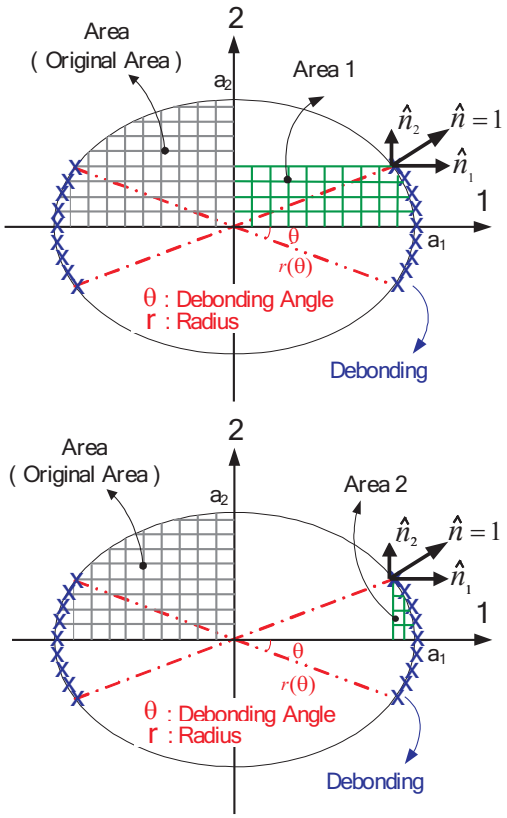

< Damage Parameter in the 1 - Direction >

$$D_1 = \frac{Area1}{Area}$$

< Damage Parameter in the 2 - Direction >

$$D_2 = \frac{Area2}{Area}$$

< Damage Parameter in the 3 - Direction >

$$D_3 = \frac{Damaged\ Arc\ Length}{Perimeter\ Length\ of\ Fiber}$$

$$Area = \frac{\pi a_1 a_2}{4}$$

$$Area1 = \frac{1}{2} a_1 \cdot \left[r\sin\theta \sqrt{1 - \frac{r^2 \sin^2\theta}{a_2^{\,2}}} + a_2 \sin^{-1}\left(\frac{r\sin\theta}{a_2} \right) \right]$$

$$Area2 = Area1 - r^2 \sin\theta \cdot \cos\theta$$

$$Damaged\ Arc\ Length = \int_0^{\theta} \sqrt{\frac{4a_1^{\,2}a_2^{\,2}\left(a_1^{\,4} + a_2^{\,4} + (a_2^{\,4} - a_1^{\,4})\cos 2\theta\right)}{\left(a_1^{\,2} + a_2^{\,2} + (a_2^{\,2} - a_1^{\,2})\cos 2\theta\right)^3}}\, d\theta$$

$$Perimeter\ Length\ of\ Fiber = \int_0^{\pi/2} \sqrt{\frac{4a_1^{\,2}a_2^{\,2}\left(a_1^{\,4} + a_2^{\,4} + (a_2^{\,4} - a_1^{\,4})\cos 2\theta\right)}{\left(a_1^{\,2} + a_2^{\,2} + (a_2^{\,2} - a_1^{\,2})\cos 2\theta\right)^3}}\, d\theta$$

Figure 1: The interfacial debonding geometry and the damage parameters for an elliptical fiber, with a_1 and a_2 denoting the principal semi-axes and r denoting the radius.

derived as

$$\theta = \sin^{-1} \sqrt{\frac{\sigma_{11}^{Interface} - \sigma_{cri}}{\sigma_{11}^{Interface} - \sigma_{22}^{Interface} \cdot \left(\frac{a_1}{a_2}\right)^4 - \sigma_{cri}\left(1 - \left(\frac{a_1}{a_2}\right)^4\right)}} \tag{21}$$

Mode 3: $\sigma_{11}^{Interface} > \sigma_{22}^{Interface} > \sigma_{cri}$

Both radial stresses in the 1- and 2-direction are greater than the critical debonding stress. In this case, for simplicity, it is assumed that the fiber is totally separated from the matrix. Accordingly, the elliptical fiber can be approximated as an elliptical microvoid.

For the above three interfacial damage modes, the range of debonding angles is between 0^o and 90^o. The lower and upper bounds of the debonding angles of a certain radial direction correspond to the perfect bonding ($\theta = 0^o$) and complete debonding ($\theta = 90^o$), respectively. To quantify the interfacial damage, the ratios of the projected damaged areas in certain directions are considered for the directional damage parameters. *Figure 1* shows the interfacial debonding geometry and the damage parameters for an elliptical fiber. The area of a quarter elliptical fiber is $Area = \pi a_1 a_2/4$; the projected damaged areas along the 1- and 2-direction are:

$$Area1 = \frac{1}{2}a_1 \left[r\sin\theta\sqrt{1 - \frac{r^2\sin^2\theta}{a_2^2}} + a_2 \sin^{-1}\left(\frac{r\sin\theta}{a_2}\right)\right] \tag{22}$$

$$Area2 = Area1 - r^2\sin\theta\cos\theta \tag{23}$$

The damaged arc length and the perimeter length of the fiber read:

$$Damaged\ arc\ length = 2a_1a_2\int_0^{\theta}\sqrt{\frac{a_1^4 + a_2^4 + (a_2^4 - a_1^4)\cos 2\theta}{(a_1^2 + a_2^2 + (a_2^2 - a_1^2)\cos 2\theta)^3}}d\theta \tag{24}$$

$$Perimeter\ arc\ length = 2a_1a_2\int_0^{\pi/2}\sqrt{\frac{a_1^4 + a_2^4 + (a_2^4 - a_1^4)\cos 2\theta}{(a_1^2 + a_2^2 + (a_2^2 - a_1^2)\cos 2\theta)^3}}d\theta \tag{25}$$

The three directional damage parameters take the form:

$$D_1 = \frac{Area1}{Area};\quad D_2 = \frac{Area2}{Area};\quad D_3 = \frac{Damaged\ Arc\ Length}{Perimeter\ Length\ of\ Fiber} \tag{26}$$

On the basis of the above damage parameters and the concept of equivalent inclusion, partially debonded isotropic fibers (Mode-2) can be replaced by perfectly bonded, orthotropic fibers with reduced elastic moduli as follows:

$$C_{ijkl}^{(2)} = \lambda_{IK}^{(2)}\delta_{ij}\delta_{kl} + \mu_{IJ}^{(2)}(\delta_{ik}\delta_{jl} + \delta_{il}\delta_{jk}),\ i,j,k,l = 1,2,3 \text{ and } I,J,K = 1,2,3 \tag{27}$$

where

$$\lambda_{IK}^{(2)} = \lambda^{1)}(\mathbf{1} - D_I)\cdot(\mathbf{1} - D_K);\quad \mu_{IJ}^{(2)} = \mu^{(1)}(\mathbf{1} - D_I)\cdot(\mathbf{1} - D_J) \tag{28}$$

Here, Mura's (1987) tensorial indicial notation is adopted; i.e., the repeated lower-case indices are summed up from 1 to 3, whereas the upper-case indices take on the same numbers as the corresponding lower-case ones but these are not summed up.

2.2 The multi-stage volume fraction evolution of debonded fibers

To characterize the evolution of interfacial damage and the transition between the three debonding modes, the volume fraction of each damage mode is expressed as follows:

$$\begin{array}{lrcl} \text{Mode 1 (no debonding)} & : \phi^{(1)} & = & \phi^{Total}(1 - P_{partial}) \\ \text{Mode 2 (partial debonding)} & : \phi^{(2)} & = & \phi^{Total}(P_{partial} - P_{complete}) \\ \text{Mode 3 (complete debonding)} & : \phi^{(3)} & = & \phi^{Total}(P_{complete}) \end{array} \tag{29}$$

where ϕ^{Total} is the volume fraction of the original (perfectly bonded) fibers in the metal matrix composite. The probabilistic functions $P_{partial}$ and $P_{complete}$ control the evolution of the volume fraction of perfectly-bonded fibers toward the 1- and the 2-direction, respectively. A Weibull distribution function is adopted to describe the partial interfacial damage evolution process:

$$P_{partial} = \mathbf{1} - \exp\left[-\left(\frac{\sigma_{11}^{Interface} - \sigma_{cri}}{S_0}\right)^M\right] \quad \texttt{for} \quad \sigma_{11}^{Interface} > \sigma_{cri} \tag{30}$$

Here, the Weibull parameters M, S_0 signify the evolution rate of the volume fractions of debonded fibers and the average interfacial strength, respectively. The parameter σ_{cri} represents the critical interfacial debonding strength between the fiber and matrix.

In our previous study, we assume that when the radial interface-stress in the 2-direction reaches the critical value, complete debonding occurs; namely, $\sigma_{11}^{Interface} > \sigma_{22}^{Interface} > \sigma_{cri}$. However, in terms of probability, the larger the debonding angle, the more likely partial debonding leads to complete debonding. In addition, when the debonding angle is 90^o, the probability for partial debonding should be equal to that for complete debonding; namely $P_{partial} = P_{complete}$. Considering the probable situation with respect to the debonding angle θ, we consider that the probability function $P_{complete}$ may be a function of the debonding angle θ and $P_{partial}$ (cf. *Figures 2*). Therefore, it is assumed that the probability function $P_{complete}$ is given as

$$P_{complete} = P_{partial} \cdot \left[\frac{1}{2}\left(1 + \sin(2\theta - \frac{\pi}{2})\right)\right] \tag{31}$$

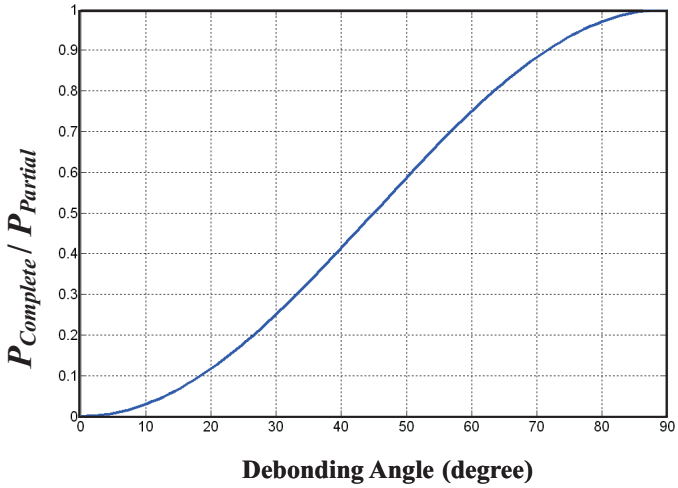

Figure 2: The probability function $P_{complete}$.

3 Effective elastoplastic-damage behavior

3.1 Effective elastic-damage moduli of four-phase composites

By using the equivalent elastic stiffness of partially debonded fibers in Eq.(27) and the evolutionary volume fractions associated with different phases of debonded fibers, the effective elastic-damage moduli of fiber reinforced composites can be predicted within the framework of micromechanics and homogenization. Since the self-equilibrium residual stresses do not influence the elastic properties of composites, the first-order formulation for fiber interactions gives the effective tangent stiffness tensor of four-phase composites:

$$\bar{\sigma} = \mathbf{C}^*\colon \bar{\varepsilon}^{\mathbf{e}} \tag{32}$$

where

$$\begin{aligned} \mathbf{C}^* &= \mathbf{C}_0 \bullet \left[\mathbf{I} + (\bar{\mathbf{Y}}^{-1} - \mathbf{S})^{-1}\right] \\ \bar{\mathbf{Y}} &= \phi^{(1)}(\mathbf{A}_1+\mathbf{S})^{-1} + \phi^{(2)}(\mathbf{A}_2+\mathbf{S})^{-1} + \phi^{(3)}(\mathbf{A}_3+\mathbf{S})^{-1} \\ \mathbf{A}_r &= (\mathbf{C}^{(r)} - \mathbf{C}_0)^{-1} \bullet \mathbf{C}_0\,, \qquad r = 1,2 \\ \mathbf{A}_3 &= -\mathbf{I} \end{aligned} \tag{33}$$

The inversion and contraction of anisotropic 4^{th}-rank tensors can be readily performed using the generalized isotropic tensorial formulas proposed by Ju and Sun (2001), and Sun and Ju (2001).

3.2 The effective yield function of multi-phase elastoplastic composites with damage and residual stress

The stress and strain fields in the matrix material vary substantially from one point to another. For instance, around the interface between the matrix and inclusion, high stress concentration occurs due to the mismatched stiffness of those materials (Christman et al., 1989a,b). As a result, the matrix material tends to yield at a relatively low stress around the interface. However, this local plastic yielding does not control the onset of global yielding. The overall yield stress of metal matrix composites is governed not so much by the premature local yielding of the matrix, but rather by the attainment of an average stress in the matrix that is sufficient for the global yielding (Clyne and Withers, 1993). Moreover, due to the similarity of the yield criteria developed for monolithic materials which reflect the triaxial state of stress, it seems reasonable to take this tri-axial state of the stress into account for metal matrix composites. A number of models use the von Mises and Tresca type yield criterion. They assume that when the average stress in the matrix exceeds the threshold value, the overall plastic flow of the composite occurs. Therefore, the matrix material plays a crucial role for the overall composite yielding (Nieh and Chellman, 1984).

In our micromechanical framework, the local stress field in the matrix point $\mathbf{x}$ is directly computed with the exterior-point Eshelby's tensor $\bar{\mathbf{G}}$ (cf. Mura, 1987; Ju and Sun, 1999) and the first-order micromechanical approximation (Ju and Chen, 1994a,b,c) as follows:

$$\sigma(\mathbf{x}|\mathbf{x}_r) = \mathbf{M}(\mathbf{x}|\mathbf{x}_r) : \sigma^o + \mathbf{N}(\mathbf{x}|\mathbf{x}_r) : \varepsilon^*_{Th} \tag{34}$$

where $\mathbf{x}_r$ denotes the center of a r^{th}-phase fiber ($r = 1, 2, 3$), and the fourth-rank tensors $\mathbf{M}(\mathbf{x}|\mathbf{x}_r)$ and $\mathbf{N}(\mathbf{x}|\mathbf{x}_r)$read

$$\mathbf{M}(\mathbf{x}|\mathbf{x}_r) \;=\; \mathbf{I} \;-\; \mathbf{C}_0 \bullet \bar{\mathbf{G}}(\mathbf{x}|\mathbf{x}_r) \bullet (\mathbf{A}_r + \mathbf{S})^{-1} \bullet \mathbf{C}_0^{-1} \tag{35}$$

$$\mathbf{N}(\mathbf{x}|\mathbf{x}_r) = \mathbf{C}_0 \bullet \bar{\mathbf{G}}(\mathbf{x}|\mathbf{x}_r) \bullet (\mathbf{A}_r + \mathbf{S})^{-1} \bullet \mathbf{B}_r \tag{36}$$

where

$$\begin{array}{l} \mathbf{B}_r = (\mathbf{C}_r - \mathbf{C}_0^{-1} \bullet \mathbf{C}_r, \quad r = 1, 2 \\ \mathbf{B}_3 = \mathbf{0} \end{array} \tag{37}$$

Here, σ^o signifies the far-field (uniform) stress field. It is noted that, similar to the interface stress given by Eq.(14), the temperature change or thermal eigenstrain affects the stress field in the matrix phase. If the thermal effect is neglected, Eq.(34) reduces to the local stress field in the matrix as expected. Further, $\bar{\mathbf{G}}$ in Eqs.(35)-(36) signifies the exterior-point Eshelby tensor which has been explicitly derived in tensor form by Ju and Yanase (2007) for an elliptical fiber.

On the basis of Eq.(34), the ensemble-area-averaging method can be directly employed to obtain the effective yield function for fiber reinforced metal matrix

composites with evolutionary multi-level damage. We adopt the commonly used von Mises yield criterion with an isotropic hardening law for illustration. Extension to more general yield criterion and general hardening law can be derived similarly with added effort. Furthermore, we consider small strain and hence the statistical microstructure of fibers embedded in a ductile matrix remains essentially unchanged. As mentioned before, the premature local matrix yielding does not necessarily govern the composite yielding. Instead, the stress field in the matrix as a whole needs to satisfy the yield criterion for the overall composite yielding.

The effective yield function for the composites proposed by Ju and Chen (1994c), and Ju, Ko and Ruan (2006, 2008) accounts for this phenomenon:

$$\bar{F} = \sqrt{\langle H \rangle_m (\mathbf{x})} - K(\bar{e}^P) \leqslant 0 \tag{38}$$

The ensemble-area-averaged stress norm $\langle H \rangle_m (\mathbf{x})$ for the composites with three distinct phases of fibers can be approximately obtained by neglecting the near-field interactions among neighboring elliptical fibers under the generalized plane-strain condition ($\bar{\varepsilon}_{33} = 0$):

$$\langle H \rangle_m (\mathbf{x}) \cong H^o + \sum_{r=1}^{3} \int_{|x-x_r| \notin \Omega_r} \{H(x|x_r) - H^o\} P(\mathbf{x}_r) dx \tag{39}$$

where x_1, x_2 and x_3 represent a material point in the perfectly bonded, partially debonded and completely debonded elliptical fibers, respectively; cf. Ju and Lee (2000), and Ju and Zhang (1998, 2001). Here, $H(\sigma) \equiv \sigma : \mathbf{I}_d : \sigma$ denotes the square of the deviatoric stress form, where $\mathbf{I}_d$ signifies the deviatoric part of the fourth-rank identity tensor $\mathbf{I}$; $H^o = \sigma^o : \mathbf{I}_d : \sigma^o$ is the square of the far-field stress norm in the matrix. Further, $P(\mathrm{x}_r)$ defines the probability density function for finding an elliptical fiber centered at x_r, and Ω_r is the domain of the r^{th}-mode elliptical fibers ($r = 1, 2, 3$). In the absence of actual microstructural evidences, $P(\mathrm{x}_r)$ is assumed to be statistically homogeneous, isotropic and uniform, thus taking the form $P(\mathrm{x}_r) = \frac{N_r}{A} = \frac{\phi^{(r)}}{\pi a_1 a_2}$, where N_r is the total number of the r^{th}-mode fibers dispersed in a representative area element A. If detailed spatial distribution of fibers can be provided, suitable probability distribution function can be implemented. In contrast to the effective medium theories (e.g., the self-consistent method, the generalized self-consistent method, the differential scheme, and the Mori-Tanaka method), where *neither* inclusion locations nor their relative configurations are taken into account, the present framework considers randomly located elliptical fibers.

In addition, in Eq.(39), the first and second terms represent the deviatoric stress norm by the far-field stress σ^o and by the perturbed stress fields in the matrix domain, respectively. Once the stress field within a matrix material point

is rendered by Eq.(34) , within a representative area element, the relationship among the normal stress components is dictated by the following equation on the basis of generalized plane strain condition for the composite ($\bar{\varepsilon}_{33} = 0$):

$$\sigma_{33} = \eta_1 \, \sigma_{11} + \eta_2 \, \sigma_{22} \tag{40}$$

where

$$\eta_1 = \frac{C^*_{1133} \cdot C^*_{2222} - C^*_{1122} \cdot C^*_{2233}}{C^*_{1111} \cdot C^*_{2222} - (C^*_{1122})^2}, \; \eta_2 = \frac{C^*_{1111} \cdot C^*_{2233} - C^*_{1133} \cdot C^*_{1122}}{C^*_{1111} \cdot C^*_{2222} - (C^*_{1122})^2} \tag{41}$$

By making use of Eqs.(34)-(35) and (40)-(41), the ensemble-area averaged current stress norm at any matrix point can be obtained as follows:

$$\langle H \rangle_m (\mathbf{x}) \cong \sigma^o \colon \mathbf{T}^A \colon \sigma^o + \mathbf{2} \cdot \sigma^o \colon \mathbf{T}^B \colon \varepsilon^*_{Th} + \varepsilon^*_{Th} \colon \mathbf{T}^C \colon \varepsilon^*_{Th} \tag{42}$$

where the components of the fourth-rank tensors $\mathbf{T}^A$, $\mathbf{T}^B$, and $\mathbf{T}^C$ can be expressed as

$$T^A_{ijkl} = K_{ijkl} +$$

$$\sum_{r=1}^{3} \left\{ \int_{\mathbf{x}_r \notin \Omega_r}^{\infty} \left(M(\mathbf{x}|\mathbf{x}_r)_{mnij} K_{mnpq} \, M(\mathbf{x}|\mathbf{x}_r)_{pqkl} - K_{ijkl} \right) P(\mathbf{x}_r) \mathbf{x}_r \right\} \tag{43}$$

$$T^B_{ijkl} = \sum_{r=1}^{3} \left\{ \int_{\mathbf{x}_r \notin \Omega_r}^{\infty} \left(M(\mathbf{x}|\mathbf{x}_r)_{mnij} \, K_{mnpq} \, N(\mathbf{x}|\mathbf{x}_r)_{pqkl} \right) P(\mathbf{x}_r) d\mathbf{x}_r \right\} \tag{44}$$

$$T^C_{ijkl} = \sum_{r=1}^{3} \left\{ \int_{\mathbf{x}_r \notin \Omega_r}^{\infty} \left(N(\mathbf{x}|\mathbf{x}_r)_{mnij} \, K_{mnpq} \, N(\mathbf{x}|\mathbf{x}_r)_{pqkl} \right) P(\mathbf{x}_r) d\mathbf{x}_r \right\} \tag{45}$$

where $i, j, k, l, m, n, p, q = 1, 2$, and

$$K_{1111} = \frac{2}{3}(\eta_1^2 - \eta_1 + 1); \quad K_{2222} = \frac{2}{3}(\eta_2^2 - \eta_2 + 1) \tag{46}$$

$$K_{1122} = K_{2211} = -\frac{1}{3}(\eta_1 + \eta_2 - 2\eta_1 \, \eta_2 + 1);$$
$$K_{1212} = K_{2121} = 1; \;\; Otherwise \; K_{ijkl} = 0 \tag{47}$$

Here, unlike the "equivalent circular exclusion zone" proposed in Ju and Sun (2001), and Ju, Ko and Zhang (2008), the exact elliptical exclusion zone Ω_r and the exact exterior-point Eshelby's tensor $\bar{G}(x)$ for the elliptical fiber are employed in Eqs.(43), (44), and (45).

In addition, the far-field stress σ^o can be expressed in terms of the macroscopic stress $\bar{\sigma}$ and thermal eigenstrain as:

$$\sigma^o = \mathbf{P} \; : \; \bar{\sigma} + \mathbf{Q} : \varepsilon^*_{Th} \tag{48}$$

where the fourth-rank tensors $\mathbf{P}$ and $\mathbf{Q}$ read

$$\mathbf{P} \;=\; \mathbf{C}_0 \bullet \left\{\mathbf{I} + (\mathbf{I}-\mathbf{S}) \bullet \bar{\mathbf{Y}}\right\}^{-1} \bullet \mathbf{C}_0{}^{-1} \tag{49}$$

$$\mathbf{Q} \;=\; \mathbf{C}_0 \bullet \left\{\mathbf{I} + (\mathbf{I}-\mathbf{S}) \bullet \bar{\mathbf{Y}}\right\}^{-1} \bullet (\mathbf{I}-\mathbf{S}) \bullet \overline{\overline{\mathbf{Y}}} \tag{50}$$

with

$$\overline{\overline{\mathbf{Y}}} \;=\; \phi^{(1)}(\mathbf{A}_1{+}\mathbf{S})^{-1} \bullet \mathbf{B}_1 + \phi^{(2)}(\mathbf{A}_2{+}\mathbf{S})^{-1} \bullet \mathbf{B}_2 + \phi^{(3)}(\mathbf{A}_3{+}\mathbf{S})^{-1} \bullet \mathbf{B}_3 \tag{51}$$

When fibers are closely packed in composites, the effect of fiber-interactions becomes significant. For example, two circular fibers separated by a center-to-center distance of less than $3a$ ($\phi \cong 34\%$, a= radius of the circular fiber) produce significant interaction. Therefore, stress concentrations and distributions in composites depend not only on the elastic properties of fibers and matrix, but also on the volume fraction and distribution of fibers. The complete state of stresses in the matrix phase may be obtained by numerical solutions such as the finite element methods (e.g., Agarwal and Broutman, 1990). Further, Ju and Chen (1994a,b) and Ju and Zhang (1998, 2001) developed higher-order micromechanical ensemble-averaged field equations. However, in the foregoing derivations, primarily to minimize mathematical complexity, the first-order micromechanical formulation is adopted. The first-order formulation provides better estimates for the effective properties of composites than the dilute solution such as the Eshelby method. Here, by virtue of mathematical simplification, a coefficient γ is introduced to account for effects of direct fiber-interactions. Accordingly, by following Eq.(18), Eq.(48) becomes:

$$\sigma^o = \gamma \cdot \mathbf{P} \;:\; \bar{\sigma} + \mathbf{Q} : \varepsilon^*_{Th} \tag{52}$$

In this study, γ is taken as 1.1 for illustration. Hence, Eqs.(42) and (52) lead to the expression:

$$\langle H \rangle_m (\mathbf{x}) = \bar{\sigma} : \bar{\mathbf{T}}^A \colon \bar{\sigma} + \mathbf{2} \cdot \bar{\sigma} : \bar{\mathbf{T}}^B \colon \varepsilon^*_{Th} + \varepsilon^*_{Th} \colon \bar{\mathbf{T}}^C \colon \varepsilon^*_{Th} \tag{53}$$

where

$$\bar{T}^A_{ijkl} = \gamma^2 P_{mnij}\, T^A_{mnpq}\, P_{pqkl} \tag{54}$$

$$\bar{T}^B_{ijkl} = \gamma P_{mnij}\, T^A_{mnpq}\, Q_{pqkl} + \gamma P_{mnij}\, T^B_{mnkl} \tag{55}$$

$$\bar{T}^C_{ijkl} = 2\, Q_{mnij}\, T^B_{mnkl} + T^C_{ijkl}; \quad (i,j,k,l,m,n,p,q = 1,2) \tag{56}$$

It is noted that, in Eq.(53), the fourth-rank tensor $\bar{\mathbf{T}}^A \equiv \mathbf{P}^{\mathbf{T}} \;:\; \mathbf{T}^A \colon \mathbf{P}$ will reduce to the classical J_2-invariant for $\phi^{(1)} = \phi^{(2)} = \phi^{(3)} = 0$, and $\gamma = 1.0$ (i.e., the matrix-only material).

Finally, the ensemble-area-averaged current stress norm for a four-phase composite is defined as:

$$\sqrt{\langle H \rangle (\mathbf{x})} = (1-\phi^{(1)}) \sqrt{\bar{\sigma} : \bar{\mathbf{T}}^A : \bar{\sigma} + \mathbf{2} \cdot \bar{\sigma} : \bar{\mathbf{T}}^B : \varepsilon^*_{Th} + \varepsilon^*_{Th} : \bar{\mathbf{T}}^C : \varepsilon^*_{Th}} \tag{57}$$

where $\phi^{(1)}$ is the perfectly bonded fiber volume fraction at the current loading. The effective yield function for the four-phase fiber reinforced ductile matrix composite can be written as

$$\bar{F} = (1-\phi^{(1)}) \sqrt{\bar{\sigma} : \bar{\mathbf{T}}^A : \bar{\sigma} + \mathbf{2} \cdot \bar{\sigma} : \bar{\mathbf{T}}^B : \varepsilon^*_{Th} + \varepsilon^*_{Th} : \bar{\mathbf{T}}^C : \varepsilon^*_{Th}} - K(\bar{e}^P) \tag{58}$$

with the isotropic hardening function $K(\bar{e}^p)$ for the four-phase composites. For simplicity, we assume that the overall flow rule for the composite is associative. In general, the overall flow rule of the composite may become *non-associative* when fibers exist according to dislocation dynamics. Extension to the non-associative flow rule can be constructed in a similar manner, but involving the normal and tangential flow directions. The effective yield function in Eq.(58) is *pressure dependent* and not of the von Mises type anymore.

Following Ju and Chen (1994c), and Ju and Zhang (2001), the effective ensemble-area averaged plastic strain rate $\dot{\bar{\varepsilon}}^{\mathbf{P}}$ and the effective plastic strain rate $\dot{\bar{e}}^P$ are defined as

$$\dot{\bar{\varepsilon}}^P = \dot{\lambda} \frac{\partial \bar{F}}{\partial \bar{\sigma}} = (1-\phi^{(1)})\, \dot{\lambda} \left(\frac{\bar{\mathbf{T}}^A : \bar{\sigma} + \bar{\mathbf{T}}^B : \varepsilon^*_{Th}}{\sqrt{\bar{\sigma} : \bar{\mathbf{T}}^A : \bar{\sigma} + \mathbf{2} \cdot \bar{\sigma} : \bar{\mathbf{T}}^B : \varepsilon^*_{Th} + \varepsilon^*_{Th} : \bar{\mathbf{T}}^C : \varepsilon^*_{Th}}} \right) \tag{59}$$

$$\dot{\bar{e}}^P = \sqrt{\frac{2}{3} \dot{\bar{\varepsilon}}^P_{ij} \dot{\bar{\varepsilon}}^P_{ij}} \tag{60}$$

For illustration, the isotropic hardening function is considered here:

$$K(\bar{e}^P) = \sqrt{\frac{2}{3}} \left\{ \sigma_y + h(\bar{e}^P)^q \right\} \tag{61}$$

where h and q define the linear and exponential isotropic hardening parameters, respectively, for the four-phase composite. It is straightforward to extend the proposed model to accommodate the kinematic hardening. Moreover, σ_y is taken as the initial *matrix* yield stress.

4 Overall elastoplastic-damage stress-strain responses

To illustrate the proposed micromechanical elastoplastic-damage model for elliptical fiber MMCs, we consider the examples of *biaxial* tensile loading under the

plane-strain condition. The applied macroscopic stress $\bar{\sigma}$ and prescribed thermal eigenstrain ε^*_{Th} can be expressed as

$$\bar{\sigma}_{11} > 0,\ \bar{\sigma}_{22} = R\,\bar{\sigma}_{11},\ \bar{\sigma}_{33} = (\eta_1 + R\,\eta_2)\,\bar{\sigma}_{11}, \quad \texttt{all other} \quad \bar{\sigma}_{ij} = 0. \tag{62}$$

$$\varepsilon^*_{Th(11)} = \varepsilon^*_{Th(22)} = \varepsilon_T$$

Here, R is a parameter of loading *stress ratio*. Specifically, if $R = 0$, the biaxial tensile loading will reduce to the uniaxial tensile loading. With the isotropic hardening law described by Eq.(61), the overall yield function becomes

$$\bar{F}(\bar{\sigma}_{11},\,\bar{e}^p) = (1-\phi^{(1)})\sqrt{\bar{\sigma} : \bar{\mathbf{T}}^A\colon \bar{\sigma} + \mathbf{2}\cdot\bar{\sigma} : \bar{\mathbf{T}}^B\colon \varepsilon^*_{Th} + \varepsilon^*_{Th}\colon \bar{\mathbf{T}}^C\colon \varepsilon^*_{Th}} -$$

$$\sqrt{\frac{2}{3}}\,\{\sigma_y + h(\bar{e}^p)^q\} \tag{63}$$

Substituting Eq.(62) into (63), the effective yield function for the case of biaxial loading reads

$$\bar{F}\,(\bar{\sigma}_{11},\,\bar{e}^p) \;=\; (1-\phi^{(1)})\;\Psi(\bar{\sigma}_{11}) - \sqrt{\frac{2}{3}}\;\{\sigma_y + h(\bar{e}^p)^q\} \tag{64}$$

where

$$\Psi(\bar{\sigma}_{11}) = \sqrt{\Psi^A + \Psi^B + \Psi^C} \tag{65}$$

with

$$\Psi^A = \left\{\bar{T}^A_{1111} + R(\bar{T}^A_{1122} + \bar{T}^A_{2211}) + R^2\bar{T}^A_{2222}\right\}\bar{\sigma}^2_{11} \tag{66}$$

$$\Psi^B = \left\{2\bar{T}^B_{1111} + 2\bar{T}^B_{1122} + 2R(\bar{T}^B_{2211} + \bar{T}^B_{2222})\right\}(\bar{\sigma}_{11}\cdot\varepsilon_T) \tag{67}$$

$$\Psi^C = \left\{\bar{T}^C_{1111} + \bar{T}^C_{1122} + \bar{T}^C_{2211} + \bar{T}^C_{2222}\right\}\varepsilon^2_T \tag{68}$$

The macroscopic incremental plastic strain rate defined by Eq.(59) becomes

$$\Delta\bar{\varepsilon}^p = \begin{bmatrix} \Delta\bar{\varepsilon}^p_{11} \\ \Delta\bar{\varepsilon}^p_{22} \end{bmatrix} = (1-\phi^{(1)})\frac{\Delta\lambda}{\Psi(\bar{\sigma}_{11})} \tag{69}$$
$$\left\{\begin{bmatrix} (\bar{T}^A_{1111} + R\bar{T}^A_{1111}) \\ (\bar{T}^A_{2211} + R\bar{T}^A_{2222}) \end{bmatrix}\bar{\sigma}_{11} + \begin{bmatrix} \bar{T}^B_{1111} + \bar{T}^B_{1122} \\ \bar{T}^B_{2211} + \bar{T}^B_{2222} \end{bmatrix}\varepsilon_T\right\}$$

for any stress beyond the initial yielding. The macroscopic incremental elastic strain is

$$\Delta\bar{\varepsilon}^e = \begin{bmatrix} \Delta\bar{\varepsilon}^e_{11} \\ \Delta\bar{\varepsilon}^e_{22} \end{bmatrix} = \begin{bmatrix} D^*_{11} + RD^*_{12} + (\eta_1 + R\eta_2)D^*_{13} \\ D^*_{12} + RD^*_{22} + (\eta_1 + R\eta_2)D^*_{23} \end{bmatrix}\Delta\bar{\sigma}_{11} \tag{70}$$

where $[D^*_{ij}] = [C^*_{ij}]^{-1}$ is the effective elastic compliance matrix in Voigt notation.

For the monotonic plane-strain biaxial tensile loading, the overall incremental macroscopic stress-strain relation can be obtained by summing Eqs.(69) and (70):

$$\Delta\bar{\varepsilon} \;=\; \left[\begin{array}{c}\Delta\bar{\varepsilon}_{11}\\ \Delta\bar{\varepsilon}_{22}\end{array}\right] = \left[\begin{array}{c} D^*_{11}+R\,D^*_{12}+(\eta_1+R\,\eta_2)\,D^*_{13}\\ D^*_{12}+R\,D^*_{22}+(\eta_1+R\,\eta_2)\,D^*_{23}\end{array}\right]\Delta\bar{\sigma}_{11}$$

$$+(1-\phi^{(1)})\frac{\Delta\lambda}{\Psi(\bar{\sigma}_{11})}\left\{\left[\begin{array}{c}(\bar{T}^A_{1111}+R\bar{T}^A_{1111})\\ (\bar{T}^A_{2211}+R\bar{T}^A_{2222})\end{array}\right]\bar{\sigma}_{11}+\left[\begin{array}{c}\bar{T}^B_{1111}+\bar{T}^B_{1122}\\ \bar{T}^B_{2211}+\bar{T}^B_{2222}\end{array}\right]\varepsilon_T\right\} \tag{71}$$

where the positive parameter $\Delta\lambda$ is solved from the nonlinear equation obtained by enforcing the plastic consistency condition $\bar{F}=0$:

$$(1-\phi^{(1)})\;\Psi(\bar{\sigma}_{11})_{n+1}=\sqrt{\frac{2}{3}}\;\left\{\sigma_y+h\left[\bar{e}^P_n+\triangle\;\bar{e}^P_{n+1}\right]^q\right\} \tag{72}$$

Under biaxial loading, Eq.(59) reduces to

$$\dot{\bar{\varepsilon}}^P=(1-\phi^{(1)})\dot{\lambda}\left(\frac{\bar{\mathbf{T}}_A\colon\bar{\sigma}+\bar{\mathbf{T}}_B\colon\varepsilon^*_{Th}}{\sqrt{\bar{\sigma}:\bar{\mathbf{T}}_A\colon\bar{\sigma}+\mathbf{2}\cdot\bar{\sigma}:\bar{\mathbf{T}}_B\colon\varepsilon^*_{Th}+\varepsilon^*_{Th}\colon\bar{\mathbf{T}}_C\colon\varepsilon^*_{Th}}}\right)= \tag{73}$$

$$(1-\phi^{(1)})\dot{\lambda}\left[\begin{array}{c}a\\ b\end{array}\right]$$

Eqs.(72) and (73) then result in

$$(1-\phi^{(1)})\Psi(\bar{\sigma}_{11})_{n+1}=\sqrt{\frac{2}{3}}\left\{\sigma_y+h\left[\bar{e}^P_n+(1-\phi^{(1)})\;\triangle\;\lambda\sqrt{\frac{2}{3}(a^2+b^2)}\right]^q\right\} \tag{74}$$

Therefore, the expression for $\triangle\;\lambda$ becomes

$$\triangle\;\lambda=\frac{1}{(1-\phi^{(1)})\sqrt{\frac{2}{3}(a^2+b^2)}}\left\{\left[\frac{\sqrt{\frac{3}{2}}(1-\phi^{(1)})\cdot\Psi(\bar{\sigma}_{11})_{n+1}-\sigma_y}{h}\right]^{1/q}-\bar{e}^p_n\right\} \tag{75}$$

5 Numerical simulations

To demonstrate the potential of proposed formulations, comparisons are made between the present theoretical predictions and the experimental data as cited by Nimmer et al. (1991). The experimental data were observed for Ti-6Al-4V matrix composites reinforced by unidirectionally aligned silicon-carbide (SiC) fibers under uniaxial transverse tensile loading. As pointed out in the literature, it is well known that the titanium composites have negligibly small interface strength (cf. Marshall et al., 1994; Gundel et al., 1995). Moreover, numerical and analytical studies of

the stress state at the interfaces indicate that interface debonding occurs at the stress levels where the applied stresses just overcome the thermal residual (radial compressive) stresses at the interface, thereby indicating the interface strength is nearly zero. Accordingly, following Warrier et al. (1997) and Naboulsi et al. (2003), the interfacial debonding criteria for the titanium composites are given under the assumption of zero interface strength as follows:

$$\begin{aligned} &\sigma^{Interface} \geqslant \sigma_{cri} = 0, \texttt{ then the interface is debonded.} \\ &\sigma^{Interface} < \sigma_{cri} = 0, \texttt{ then the interface is perfectly bonded.} \end{aligned} \tag{76}$$

Furthermore, the study on SiC fiber reinforced titanium-matrix composites shows that an elastoplastic model can predict similar residual stress as a viscoelastic/viscoplastic model if the reference temperature is selected as 0.7-0.8 times the absolute processing temperature (Kroupa et al., 1994; Warrier et al., 1997). Moreover, during the early cool-down period following the fabrication, thermal residual stresses generated in the composites may be quickly relaxed out (Saigal et al., 1992). Therefore, since the viscoelastic/viscoplastic analysis is not performed in the present analysis, the temperature changes are taken as 700 ^{o}C (T = 23^{o}C) and 480 ^{o}C (T = 315^{o}C), which are lower than the actual temperature changes.

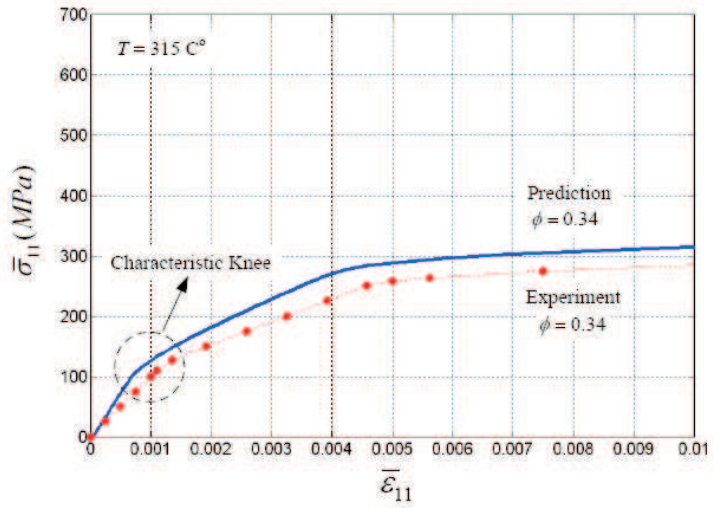

Matrix: $E_0 = 113.7 * 10^3$ MPa, $\nu_0 = 0.3$; **Fiber**: $E_1 = 113.7 * 10^3$ MPa, $\nu_1 = 0.25$; $\sigma_y = 900$ MPa, $h = 600$ MPa, $q = 0.35$, $M = 1.0$, $S_o = 10$ MPa; $\phi = 0.34$, $T = 23^o$C, $\Delta T_{ref} = -700^o$C, $\alpha_0 = 9.44 * 10^{-6}/^o$C, $\alpha_1 = 4.86 * 10^{-6}/^o$C.

Figure 3: Comparison of present theoretical stress-strain prediction with experimental data ($T = 23^o$C) by Nimmer et al. (1991).

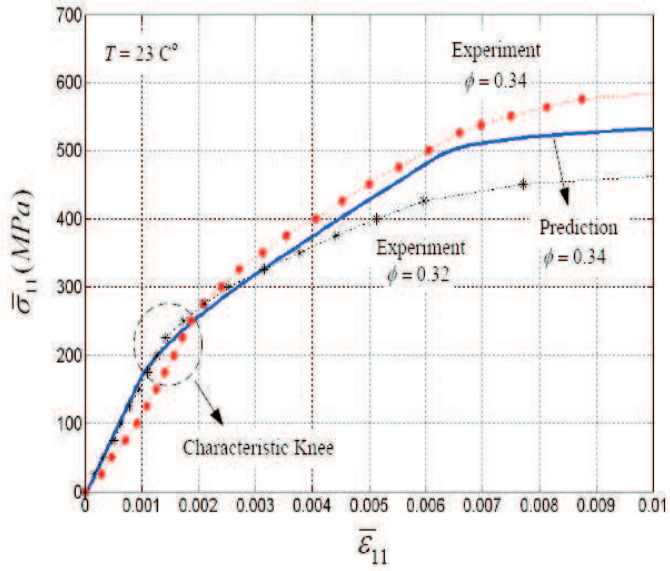

Matrix: $E_0 = 97.9 * 10^3$ MPa, $\nu_0 = 0.3$; **Fiber**: $E_1 = 414.0 * 10^3$ MPa, $\nu_1 = 0.25$;$\sigma_y = 517$ MPa, $h = 600$ MPa, $q = 0.35$, $M = 1.0$, $S_o = 10$ MPa; $\phi = 0.34$, $T = 315^o$C, $\Delta T_{ref} = -480^o$C, $\alpha_0 = 9.78 * 10^{-6}/^o$C, $\alpha_1 = 4.86 * 10^{-6}/^o$C.

Figure 4: Comparison of present theoretical stress-strain prediction with experimental data (T= 315^{o}C) by Nimmer et al. (1991).

As shown in *Figures 3* and *4*, even though zero interface strength is assumed in the theoretical prediction, the interfacial debonding cannot be observed instantly after the mechanical loading is applied; cf. *Figures 5* and *6*. Instead, the progressive interfacial debonding process is activated around the stress level of 200 MPa (T= 23^{o}C) and 100 MPa (T= 315^{o}C), exhibiting a characteristic knee in the transverse stress-strain curve. In fact, if the weak interface strength is considered, the only strong bond between the fibers and matrix is the "locking effect" due to the differential thermal contraction misfit (the cramping residual stresses) between the fibers and matrix (Hu, 1996). Further, instead of using the initial composite yield stress (Ju, Ko and Zhang., 2008), the present effective yield function in Eqs. (58)-(61) makes use of the initial matrix yield stress (900 MPa), and our theoretical predictions are in good agreement with experimental data by incorporating the thermal residual stresses at the room (T= 23^{o}C) and elevated temperature (T= 315^{o}C), respectively. Moreover, when $\phi = 0$ (the matrix-only material), the effective yield function can easily recover that for the matrix material.

Though thermal residual stresses can be beneficial, they can also be detrimental in terms of lowering the tensile composite yield strength. Prior to mechanical loading, the matrix is pre-stressed under tension due to residual stresses, which

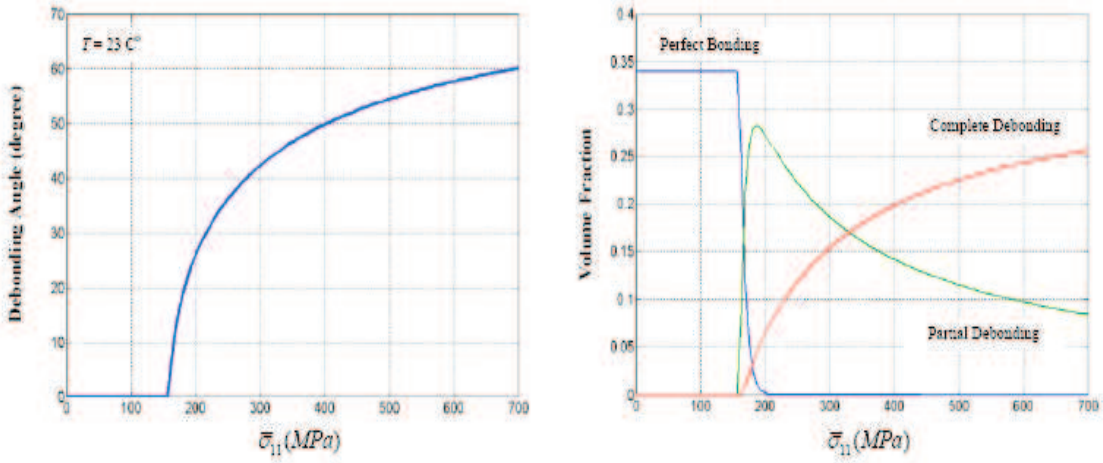

Figure 5: The theoretical predictions on the debonding angles and the volume fraction evolutions at room temperature (T= 23^{o}C).

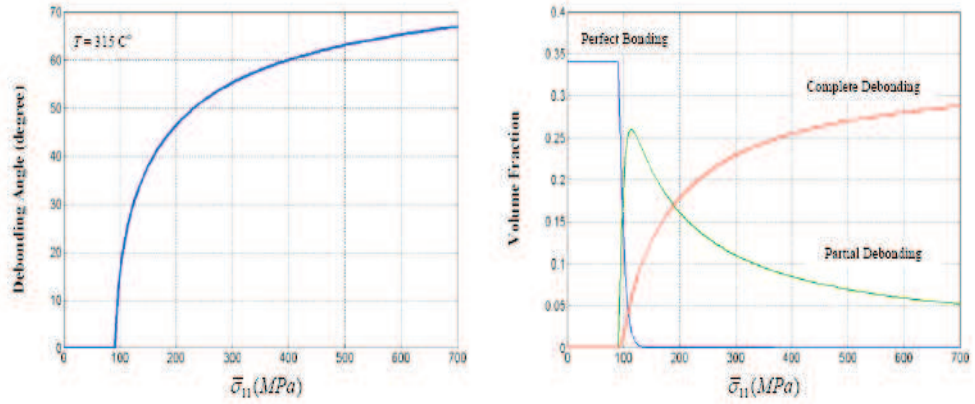

Figure 6: The theoretical predictions on the debonding angles and the volume fraction evolutions at elevated temperature (T= 315^{o}C).

superficially lower the tensile matrix yield strength. Since the matrix material has substantial effect on the composite yielding, the lower-tensile matrix yield strength leads to the lower-tensile composite yield strength as well. As rendered in *Figure 7*, the coupled effects by the interfacial damage and thermal residual stresses are significant, leading to high anisotropy in the tensile/compressive relation; e.g., the tensile composite yield strength is much lower than the compressive composite yield strength.

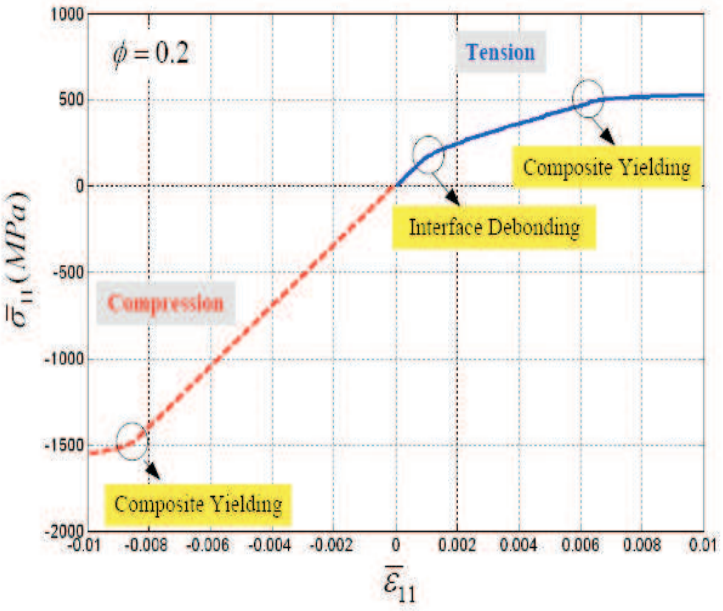

Figure 7: The tensile/compressive transverse stress-strain behavior.

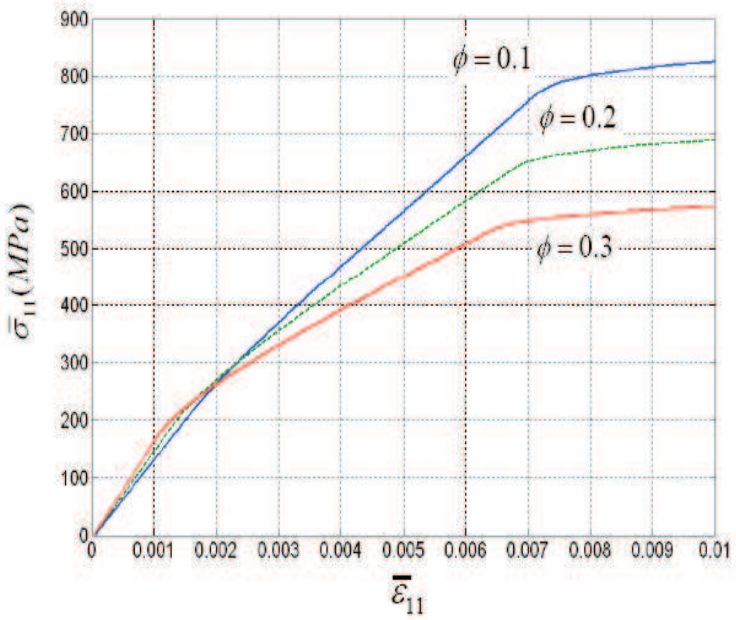

Figure 8: The effects of fiber volume fractions upon the overall stress-strain behaviors.

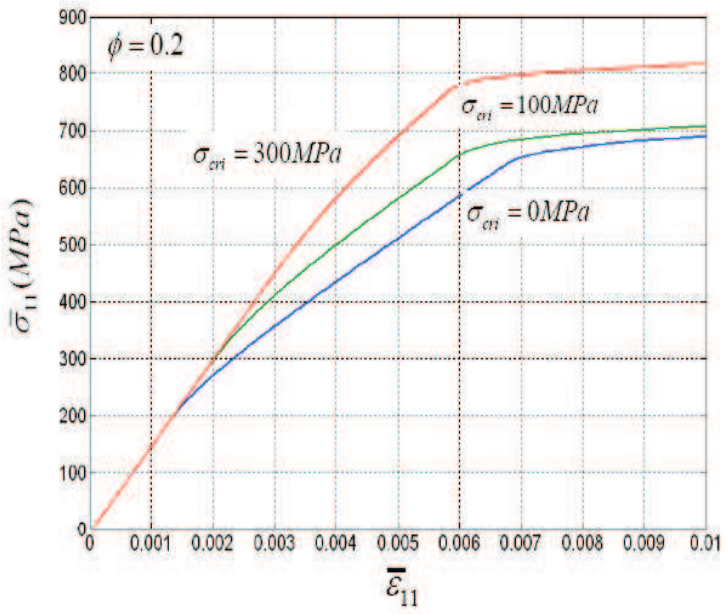

Figure 9: The effects of fiber interface strengths upon the overall stress-strain behaviors.

For a composite with weak interfaces, the fibers serve as the source of interfacial damage at the relatively low external load instead of acting as reinforcements. As *Figure 8* shows, the higher fiber volume fraction initially results in higher composite stiffness.

However, the interfacial damage gradually reduces the load transfer ability between the fibers and the matrix. Consequently, a higher volume fraction results in increased amount of damage as well as lower composite yield strength under the transverse loading. This clearly illustrates the deficiency of MMCs with weak interfaces. Even though we may improve the transverse properties of the composites using a low volume fraction of fibers, we nonetheless lose the advantage of using fiber reinforced composites. On the other hand, if we can enhance the interface strength by considering fiber coating, improved processing method or choosing different fibers/matrix, higher interface strength will lead to higher stiffness and higher composite yield strength as demonstrated by *Figure 9*.

In addition, the fiber aspect ratios have significant effects on the responses of composites under uniaxial transverse loading; cf. *Figures 10* and *11*. In contrast to the uniaxial loading case, the use of elliptical fibers does not lead to better performance of composites in the case of *biaxial* loading; cf. *Figures 12*. Since the interfacial debonding easily propagates under the biaxial tensile loading, the elliptical-fibers can easily debond at the relatively low applied load. For instance,

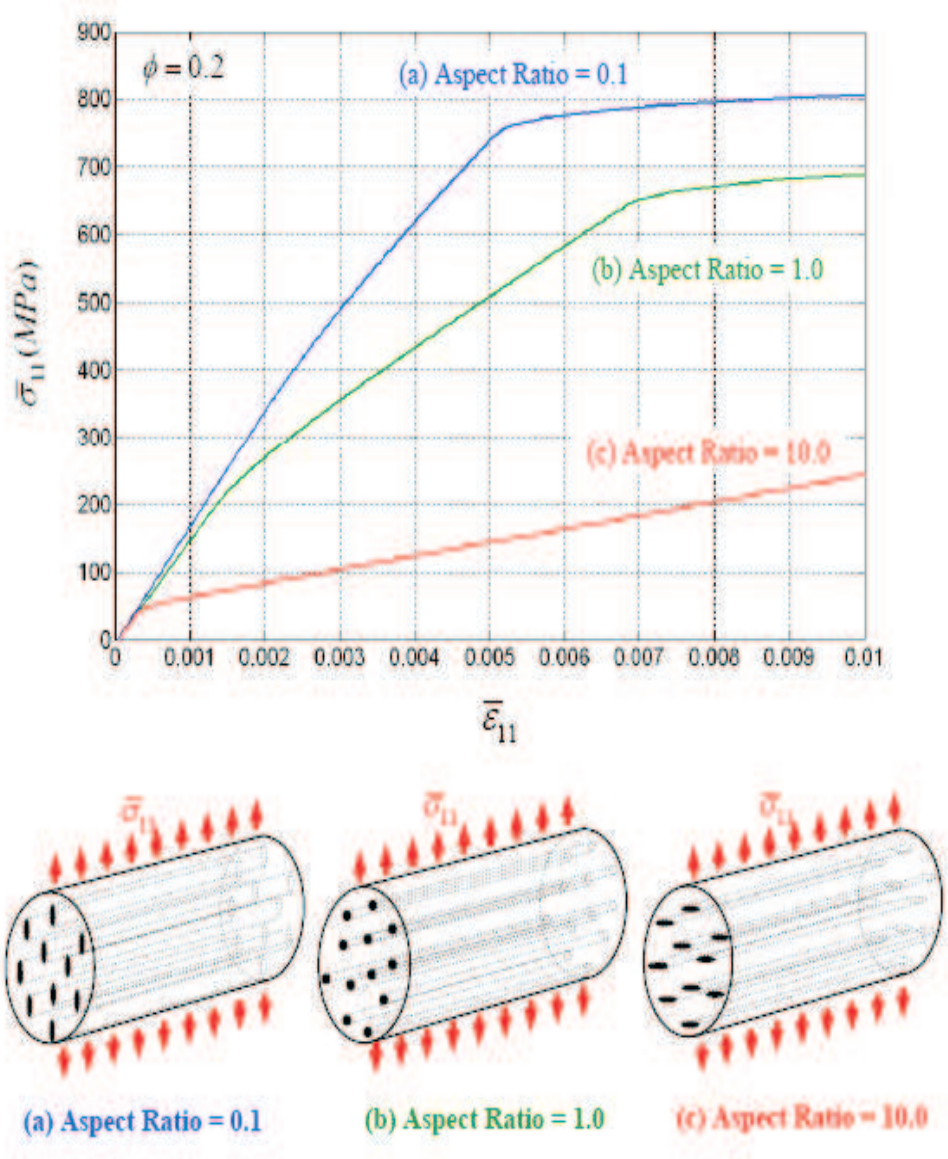

Figure 10: The effects of fiber aspect ratios upon the overall stress-strain behaviors under the uniaxial transverse tensile loading.

the overall stress-strain responses in the 2-direction exhibit lower responses with decreasing α for $R = 0.7$; cf. *Figure 12(b)*.

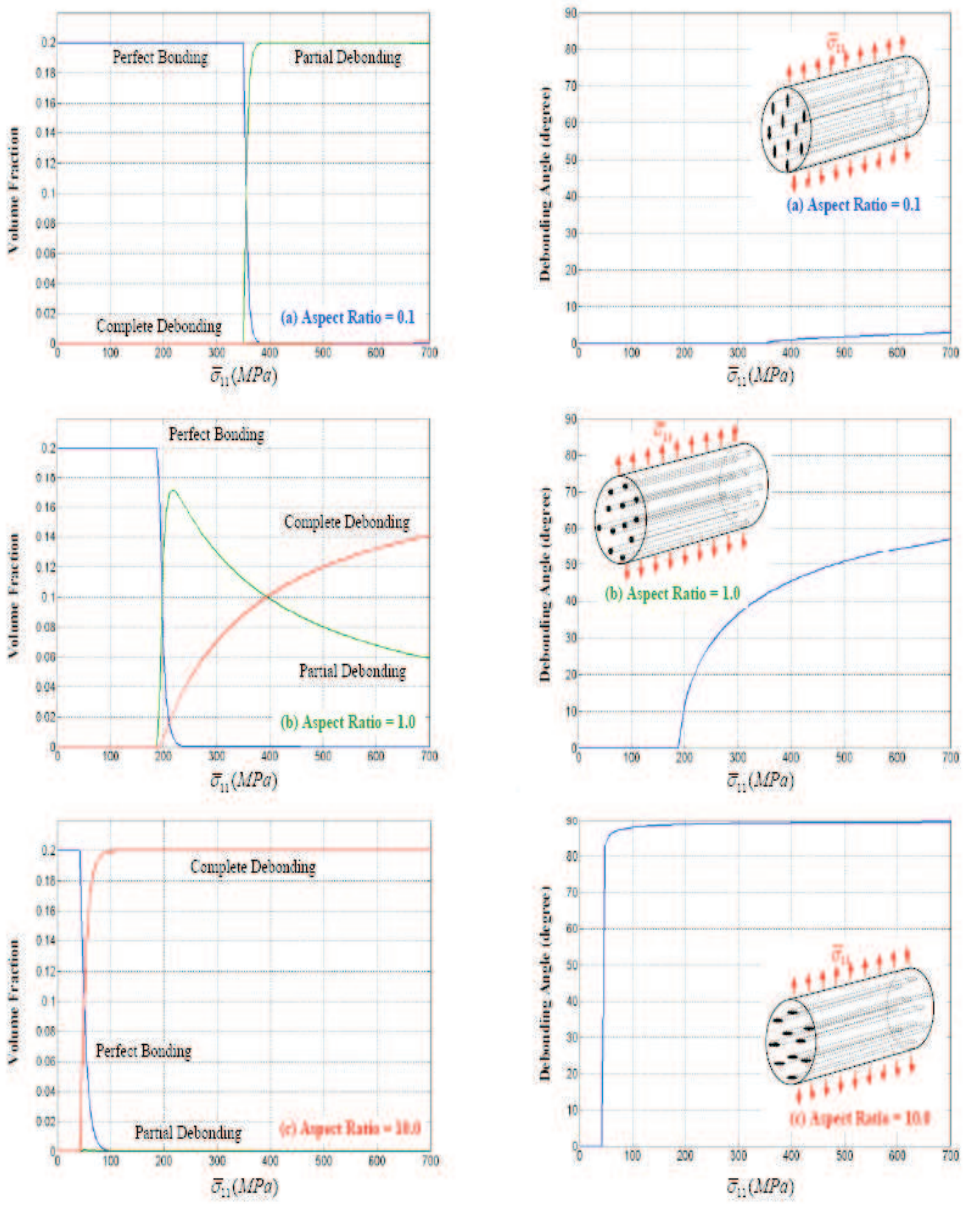

Figure 11: The effects of fiber aspect ratios upon the interfacial debonding angles and the volume fraction evolutions under the uniaxial transverse tensile loading.

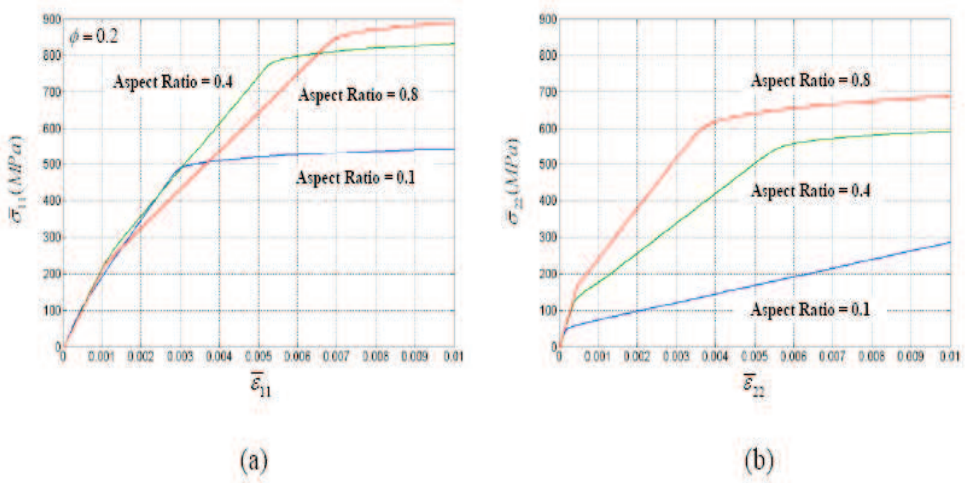

Figure 12: The effects of fiber aspect ratios upon the stress-strain behaviors under the biaxial transverse tensile loading, featuring $R = 0.7$. (a) $\overline{\sigma}_{11} vs.\ \overline{\varepsilon}_{11}$; (b) $\overline{\sigma}_{22} vs.\ \overline{\varepsilon}_{22}$.

6 Conclusions

To investigate the effects of thermal residual stresses upon the mechanical responses of continuous-fiber reinforced MMCs under the transverse loading condition, a multi-stage micromechanical elastoplastic damage formulation is proposed by incorporating the thermal eigenstrain concept and evolutionary interfacial fiber debonding. It is demonstrated that the stress fields of interfaces and matrix are composed of the mechanical and thermal components. The predicted thermomechanical behaviors of composites are consistent with the experimental observations in the literature. Moreover, the effects of elliptical fiber aspect ratios, volume fractions, interfacial strengths and biaxial stress ratios are also systematically studied.

Acknowledgments: This work is in part sponsored by the Faculty Research Grant of the Academic Senate of UCLA (Fund Number 4-592565-19914) and in part by the Bellagio Engineering.

References

[1] Aboudi, J. (1987), "Damage in composites – Modeling of imperfect Bonding", *Compos. Sci. Technol.*, **28**: 103-128.

[2] Agarwal, B.D., and Broutman, L.J. (1990), "Analysis and performance of fiber composites", John Wiley & Sons, Inc.

[3] Aghdam, M.M., and Falahatgar. S.R. (2004), "Micromechanical modeling of interface damage of metal matrix composites subjected to transverse loading", *Compos. Struct.*, **66**: 415-420.

[4] Arsenault, R.J., and Taya, M. (1987), "Thermal residual stress in metal matrix composites", *Acta Metall.*, **35**: 651-659.

[5] Christensen, R.M., and Lo, K.H. (1979) "Solutions for effective shear properties in three phase sphere and cylinder models", *J. Mech. Phys. Solids,* **27**: 315–330.

[6] Christman, T., Needleman, A., Nutt, S., and Suresh, S. (1989a), "On microstructural evolution and micromechanical modeling of deformation of a whisker-reinforced metal-matrix composite", *Mater. Sci. Eng.,* **A107**: 49-61.

[7] Christman, T., Needleman, A., Nutt, S., and Suresh, S. (1989b), "An experimental and numerical study of deformation in metal-ceramic composites", *Acta Metall.*, **37**: 3029-3050.

[8] Clyne, T.W., and Withers, P.J. (1993), "An introduction to metal matrix composites"**,** Cambridge University Press.

[9] Davis, L.C., and Allison, J.E. (1993), "Residual stresses and their effects on deformation in particle-reinforced metal-matrix composites", *Metall. Trans. A*, **24**: 2487-2496.

[10] Duan, H.L., Wang, J., Huang, Z.P., and Luo, Z.Y. (2005), "Stress concentration tensors of inhomogeneities with interface effects", *Mech. Mater.*, **37**: 723-736.

[11] Eshelby, J.D. (1957), "The determination of the elastic field of an ellipsoidal inclusion, and related problems", *Proc. R. Soc. Lond.,* **A241**: 376-396.

[12] Gao. Z. (1995), "A circular inclusion with imperfect interface: Eshelby's tensor and related problems", *ASME J. Appl. Mech.*, **62**: 860-866.

[13] Ghahremani, F. (1980), "Effect of grain boundary sliding on anelasticity of polycrystals", *Int. J. Solids & Struct.*, **16**: 825-845.

[14] Gundel, D.B., Majumdar, B.S., and Miracle, D.B. (1995), "Evaluation of the transverse response of fiber-reinforced composites using a cross shaped sample geometry", *Scripta Metall. Mater.,* **33**: 2057-2065.

[15] Gundel, D.B., Warrier, S.G., and Miracle, D.B. (1999), "The transverse tensile behavior of SiC-fiber/Ti-6Al-4V composites 2. Stress distribution and interface failure", *Compos. Sci. Technol.,* **59**: 1087-1096.

[16] Hashin, Z. (1991), "The spherical inclusion with imperfect interface", *ASME J. Appl. Mech.*, **58**: 444-449.

[17] Hashin, Z. (2002), "Thin interface/imperfect interface in elasticity with application to coated fiber composites", *J. Mech. Phys. Solids*, **50**: 2509-2537.

[18] Hashin, Z., and Monteiro, P.J.M. (2003), "An inverse method to determine the elastic properties of the interface between the aggregate and the cement paste", *Cement & Concrete Research*, **32**: 1291-1300.

[19] Heukamp, F.H., Lemarchand, E., and Ulm, F.J. (2005), "The effect of interfacial properties on the cohesion of highly filled composite materials", *Int. J. Solids & Struct.*, **42**: 287-305.

[20] Hill, R. (1965), "A self-consistent mechanics of composite materials", *J. Mech. Phys. Solids*, **13**: 213-222.

[21] Hu, S. (1996), "The transverse failure of a single-fiber metal-matrix composite: experiment and modeling", *Compos. Sci. Technol.,* **56**: 667-676.

[22] Hu, G.K., and Weng, G.J. (1998), "Influence of thermal residual stress on the composite macroscopic behavior", *Mech. Mater.*, **27**: 229-240.

[23] Jasiuk, I., Tsuchida, E., and Mura, T. (1987), "The sliding inclusion under shear", *Int. J. Solids & Struct.*, **23**: 1373-1385.

[24] Ju, J.W. and Chen, T.M. (1994a), "Micromechanics and effective moduli of elastic composites containing randomly dispersed ellipsoidal inhomogeneities", *Acta Mech.,* **103**: 103-121.

[25] Ju, J.W., and Chen, T.M. (1994b), "Effective elastic moduli of two-phase composites containing randomly dispersed spherical inhomogeneities", *Acta Mech.,* **103**: 123-144.

[26] Ju, J.W., and Chen, T.M. (1994c), "Micromechanics and effective elastoplastic behavior of two-phase metal matrix composites', *ASME J. Eng. Mech.*, **116**: 310-318.

[27] Ju, J.W., and Ko, Y.F., (2008), "Micromechanical elastoplastic damage modeling of progressive interfacial arc debonding for fiber reinforced composites", *Int. J. Damage. Mech.*, in press.

[28] Ju, J.W., Ko, Y.F., and Ruan, H.N. (2006), "Effective elastoplastic damage mechanics for fiber-reinforced composites with evolutionary complete fiber debonding", *Int. J. Damage Mech.,* **15**: 237-265.

[29] Ju, J.W., Ko, Y.F., and Ruan, H.N. (2008), "Effective elastoplastic damage mechanics for fiber reinforced composites with evolutionary partial fiber debonding", *Int. J. Damage Mech.,* in press.

[30] Ju, J.W., Ko, Y.F., and Zhang, X.D. (2008), "Multi-level elastoplastic damage mechanics for elliptical fiber reinforced composites with evolutionally fiber debonding", *Int. J. Damage. Mech.*, in press.

[31] Ju, J.W., and Lee, H.K. (2000). "A micromechanical damage model for effective elastoplastic behavior of ductile matrix composites considering evolutionary complete particle debonding", *Comput. Methods Appl. Mech. Engng.*, **183**: 201-222.

[32] Ju, J.W., and Lee, H.K. (2001), "A micromechanical damage model for effective elastoplastic behavior of partially debonded ductile matrix composites", *Int. J. Solids & Struct.*, **38**:6307-6332.

[33] Ju, J.W., and Sun, L.Z. (1999), "A novel formulation for the exterior-point Eshelby's Tensor of an ellipsoidal inclusion", *ASME J. Applied Mech.*, **66**: 570-574.

[34] Ju, J.W., and Sun, L.Z. (2001), "Effective elastoplastic behavior of metal matrix composites containing randomly located aligned spheroidal inhomogeneities. Part I: micromechanics-based formulation", *Int. J. Solids & Struct.*, **38**: 183-201.

[35] Ju, J.W., and Yanase, K. (2007), "Micromechanical elastoplastic damage mechanics for elliptical fiber reinforced composites with progressive partial fiber debonding", *Int. J. Damage. Mech.*, accepted for publication.

[36] Ju, J.W., and Zhang, X.D. (1998), "Micromechanics and effective transverse elastic moduli of composites with randomly located aligned circular fibers", *Int. J. Solids & Struct.*, **35**: 941-960.

[37] Ju, J.W., and Zhang, X.D. (2001), "Effective elastoplastic behavior of ductile matrix composites containing randomly located aligned circular fibers", *Int. J. Solids & Struct.*, **38**: 4045-4069.

[38] Kroupa, J.L. and Nuw, R.W. (1994), "The nonisothermal viscoplastic behavior of a titanium-matrix composite", *Compos. Eng.*, **4**: 965-977.

[39] Levy, A., and Papazian, J.M. (1991), "Elastoplastic finite element analysis of short-fiber-reinforced SiC/Al composites: effect of thermal treatment", *Acta Metall. Mater.*, **39**: 2255-2266.

[40] Levy, A., and Papazian, J.M. (1993), "Finite element analysis of whisker reinforced SiC/Al composites subjected to cryogenic temperature thermal cycling", *J. Eng. Mater. Technol.*, **115**: 129-133.

[41] Li, G., Zhao, Y., and Pang, S.S. (1999), "Four-phase sphere modeling of effective bulk modulus of concrete", *Cement & Concrete Research.*, **29**: 839-845.

[42] Liu, H.T., and Sun, L.Z. (2004), "Effects of thermal residual stress on effective elastoplastic behavior of metal matrix composites", *Int. J. Solids & Struct.*, **41**: 2189-2203.

[43] Liu, H.T., Sun, L.Z., and Ju, J.W. (2004), "An interfacial debonding model for particle-reinforced composites", *Int. J. Damage Mech.*, **13**: 163-185.

[44] Liu, H.T., Sun, L.Z., and Ju, J.W. (2006), "Elastoplastic modeling of progressive interfacial debonding for particle-reinforced metal matrix composites", *Acta Mech.,* **181**: 1-17.

[45] MacLaughlin, R. (1977), "A study of the differential scheme for composite materials", *Int. J. Eng. Sci.*, **15**: 237-244.

[46] Marshall, D.B., Morris, W.L., Cox, B.N., Graves, J., Porter, J.R., Kouris, D., and Everett, R.K. (1994), "Transverse strengths and failure mechanisms in Ti_3Al matrix composites", *Acta Metall. Mater.,* **42**: 2657-2673.

[47] Mori, T., and Tanaka, K. (1973), "Average stress in matrix and average elastic energy of materials with misfitting inclusions", *Acta Metall.*, **21**: 571-574.

[48] Mura, T. (1987), "Micromechanics of defects in solids", (2^{nd} Edition), Martinus Nijhoff Publishers, Dordrecht.

[49] Mura, T., and Furuhashi, R. (1984), "The elastic inclusion with a sliding interface", *ASME J. Appl. Mech.*, **51**: 308-310.

[50] Naboulsi, S. (2003), "Modeling transversely loaded metal-matrix composites", *J. Composite Mater.,* **37**: 55-72.

[51] Nemat-Nasser, S., and Hori, M. (1993), "Micromechanics: overall properties heterogeneous materials", Elsevier Science Publisher B.V, the Netherlands.

[52] Nieh, T.G., and Chellman, D.J. (1984), "Modulus measurements in discontinuous reinforced aluminum composites", *Scripta Metall.,* **18**: 925-928.

[53] Nimmer, R.P., Bankert, R.J., Russell, E.S., Smith, G. A., and Wright P.K. (1991), "Micromechanical modeling of fiber/matrix interface effects in transversely loaded SiC/Ti-6-4 metal matrix composites", *J. Comp. Tech. & Research,* **13**: 3-13.

[54] Norris, A.N. (1985), "A differential scheme for the effective modulus of composites", *Mech. Mater.*, **4**: 1-16.

[55] Povirk, G.L., Stout, M.G., Bourke, M., Goldstone, J.A., Lawson, A.C., Lovato, M., MacEwen, S.R., Nutt, S.R., and Needleman, A. (1991), "Mechanically induced residual stresses in Al/SiC composites", *Scripta Metallurgica*, **25**: 1883-1888.

[56] Qu, J. (1993a), "The effect of slightly weakened interfaces on the overall elastic properties of composite materials", *Mech. Mater.*, **14**: 269-281.

[57] Qu, J. (1993b), "Eshelby tensor for an elastic inclusion with slightly weakened Interface", *ASME J. Appl. Mech.*, **60**: 1048-1050.

[58] Qu, J., and Cherkaoui, M. (2006), "Fundamentals of micromechanics of solids", John Wiley & Sons, Inc.

[59] Rinaldi, A., Krajcinovic, D., and Mastilovic, S. (2007), "Statistical damage mechanics and extreme value theory", *Int. J. of Damage Mech.,* **16(1)**: 57-76.

[60] Saigal, A., Kupperman, D.S., and Majumdar, S. (1992), "Residual strains in titanium matrix high-temperature composites", *Mater. Sci. Eng.*, **A150**: 59-66.

[61] Shen, H., Schiavone, P., Ru, C.Q., and Mioduchowski, A. (2000), "Analysis of internal stress in an elliptic inclusion with imperfect interface in plane elasticity", *Math. Mech. Solids*, **5**: 501-521.

[62] Sun, L.Z., and Ju, J.W. (2001), "Effective elastoplastic behavior of metal matrix composites containing randomly located aligned spheroidal inhomogeneities. Part II: applications", *Int. J. Solids & Struct.*, **38**: 203-225.

[63] Sun, L.Z., and Ju, J.W. (2004), "Elastoplastic modeling of metal matrix composites contai5ning randomly located and oriented spheroidal particles", *J. Appl. Mech.*, ASME, **71**: 774-78.

[64] Tamirisakandala, S., Bhat, R.B., and Miracle, D.B. (2004), "Powder metallurgy Ti-6Al-4V-xB alloys: processing, microstructure, and properties", *JOM (J. of the Minerals, Metals & Materials Society)*, **56**: 60-63.

[65] Warrier, S.G., Majumdar, B.S., Gundel, D.B., and Miracle, D.B. (1997), "Implication of tangential shear stress induced failure during transverse loading of SiC/Ti-6Al-4V composites", *Acta Mater.*, **8**: 3469-3480.

[66] Warrier, S.G., Rangaswamy, P., Bourke, M.A.M., and Krishnamurthy, S. (1999), "Assessment of the fiber/matrix interface bond strength in SiC/Ti-6Al-4V composites", *Mater. Sci. Eng.*, **A259**: 220-227.

[67] Weibull, W. (1951), "A statistical distribution function of wide applicability", *ASME J. Appl. Mech.*, **18**: 293-297.

[68] Weng, G.J. (1984), "Some elastic properties of reinforced solids, with special reference to isotropic ones containing spherical inclusions", *Int. J. Eng. Sci.*, **22**: 845-856.

[69] Withers, P.J., and Bhadeshia, H.K.D.H. (2001a), "Residual stress, part 1 – measurement techniques", *Mater. Sci. Technol.*, **17**: 355-365.

[70] Withers, P.J., and Bhadeshia, H.K.D.H. (2001b), "Residual stress, part 2 – nature and origins", *Mater. Sci. Technol.*, **17**: 366-375.

[71] Withers, P.J., Stobbs, W.M., and Pedersen, O.B. (1989), "The application of the Eshelby method of internal stress determination for short fibre metal matrix composites", *Acta Metall.*, **35**: 3061-3084.

[72] Zhao, Y.H., and Weng, G.J. (1997), "Transversely isotropic moduli of two partially debonded composites", *Int. J. Solids & Struct.,* **34**: 493-507.

[73] Zhao, Y.H., and Weng, G.J. (2002), "The effect of debonding angle on the reduction of effective moduli of particle and fiber-reinforced composites", *ASME J. Applied Mech.,* **69**: 292-302.

[74] Zheng, S.F., Denda, M., and Weng, G.J. (2003), "Overall elastic and elastoplastic behavior of a partially debonded fiber-reinforced composite", *J. Compos. Mater.,* **37**: 741-758.

[75] Zhong, Z., and Meguid, S.A. (1997), "On the elastic field of a spherical inhomogeneity with an imperfectly bonded interface", *J. Elasticity*, **46**: 91-113.

[76] Zhou, C., Yang, W., and Fang, D., (2000), "Damage of short-fiber-reinforced metal matrix composites considering cooling and thermal cycling", *J. Eng. Mater. Technol.*, **122**: 203-208.

Submitted on February 2008, revised on March 2008.

Elastoplastična mikromehanika oštećenja kompozita sa vlaknima eliptičnog poprečnog preseka i progresivnim delimičnim odvajanjem vlakana i termičkim zaostalim naponima

U cilju predvidjanja ukupnog transverzalnog mehaničkog ponašanja kompozita sa kontinualnim vlaknima eliptičnog poprečnog preseka i duktilnom matricom predložena je, u okviru mikromehanike i homogenizacije, formulacija na osnovi elastoplastičnog ošteenja uzimanjem u obzir oštećenja interfejsa i termičkih zaostalih napona. Pristup se zasniva na konceptu ekvivalentne inkluzije i uzima u obzir ugao progresivnog odvajanje interfejsa, pri čemu su delimično odvojena vlakna zamenjena sa ekvivalentnim, ortotropskim, idealno vezanim vlaknima. Razmatrana su tri modela oštećenja interfejsa. Veibulova funkcija gustine raspodele verovatnoće je usvojena radi opisivanja promenljivosti verovatnoće progresivnog, delimičnog odvajanja vlakana. Efektivni moduo elastičnosti četvorofaznog kompozita, koji se sastoji od duktilne matrice i nasumično rasporedjenih, ali jednoosno upravljenih, vlakana je izveden korišćenjem mikromehanike.

Zaostali termički naponi su uzeti u obzir kroz koncept termičke sopstvene specifične deformacije (eigenstrain) u cilju ispitivanja efekata napona zaostalih iz proizvodnog procesa. Korišćenjem mikromehaničke aproksimacije, ukupni naponsko-deformacioni odziv i efektivna funkcija tečenja su formulisani sa termičkom sopstvenom specifičnom deformacijom (eigenstrain). Prilikom poredjenja rezultata sa dostupnim eksperimentalnim podacima diskutovani su značajni efekti zaostalih termičkih napona. Takodje su sistematski ispitani efekti čvrstoće interfejsa i oblika poprečnog preseka vlakna na mehaničko ponašanje kompozita.

doi:10.2298/TAM0803137J Math.Subj.Class.: 74L15, 92C37